Numerical simulation of neutral gas release experiments in the ionosphere*

H. Okuda†
Plasma Physics Laboratory, Princeton University, Princeton, New Jersey 08543

Edgar Y. Choueiri
Electric Propulsion and Plasma Dynamics Laboratory, Princeton University, Princeton, New Jersey 08544

(Received 3 November 1993; accepted 12 January 1994)

A two-and-one-half-dimensional electrostatic particle simulation model has been developed to study neutral gas release experiments into the ionosphere. The electrons are assumed guiding center particles, while the full dynamics of the ions (with real masses) are followed in time and space. Ionization processes of the neutral gas by charge exchange and electron impact are included by means of the Monte Carlo technique. It is shown that the model can be used to simulate the neutral gas interaction, with the ionosphere using realistic experimental parameters. The model was applied to study the critical ionization velocity (CIV) tests recently conducted as part of the ATLAS-1 [Geophys. Res. Lett. **20**, 499 (1993)] xenon gas releases from the space shuttle. The simulation results show suprathermal electrons produced by an ion beam-driven lower hybrid instability, create a xenon ion population much more rapidly than the production by classical processes, indicating the prevalence of a CIV-type mechanism.

I. BACKGROUND AND INTRODUCTION

The interaction of a neutral gas with a plasma in a magnetic field has been studied in laboratory and space plasmas. Under certain conditions, a neutral gas undergoes a rapid ionization, leading to the creation of a highly ionized gas. The process, called the critical ionization velocity (CIV), was proposed by Alfvén[1] and is essentially an instability-driven ionization mechanism, where neutral gas is ionized in a more abrupt and efficient manner than can be accounted for by classical means (thermal electron impact, photoionization, charge stripping, charge exchange, etc.). Moreover, ionization through CIV takes place in a threshold fashion, when the kinetic energy associated with the neutral gas streaming perpendicular to the magnetic field in the background plasma exceeds the ionization potential of the neutrals. A critical velocity for anomalous ionization was therefore hypothesized by Alfvén to exist at

$$V_c = (2e\phi_{\text{ion}}/M_n)^{1/2},$$

hence, the name "critical ionization velocity." Here e is the magnitude of the electronic charge, ϕ_{ion} is the ionization potential, and M_n is the mass of a neutral particle.

Theoretical studies and observations of staged CIV interactions in the laboratory have characterized the phenomenon as one in which the free-energy source associated with the directed kinetic energy of the relative motion between two plasma components excites plasma microinstabilities of the streaming (or beam) type. These instabilities would then channel a substantial part of the relative kinetic energy to heat electrons, creating a population of electrons with energies above the ionization energy. These high-energy electrons would then contribute to an enhanced ionization process. The energy going into ionization ultimately comes from the relative motion (i.e., the beam kinetic energy), and consequently the CIV interaction results in slowing down the relative velocity to near V_c during the interaction.

The instability, typically of the lower hybrid mode, is originally ignited by the cross-streaming of "seed" charged particles in the neutral gas with respect to plasma particles and maintained through the cross-streaming between newly created and old charged particle populations. The lower hybrid wave can easily be destabilized by an ion beam perpendicular to the magnetic field when the beam velocity is above the ion thermal speed. It must be emphasized that in all CIV scenarios, a "seed" of charged particle must initially exist in the neutral gas. Such seeds could be due to any weak ionization of photonic or thermal origin, and, most likely in the case of releases in space–charge exchange collisions.

The CIV phenomenon is of direct relevance to many problems of plasma dynamics, where a plasma and a neutral gas are in relative motion and where ionization is a sizeable energy sink. Plasma problems where CIV is believed to play an important role include interaction of spacecraft exhaust with the ionosphere, plasma guns, plasma thrusters, and accelerators, spacecraft environment effects on spacecraft charging, and other more natural occurrences in space plasmas such as cometary coma and comet tail formation. Theory, simulation, and laboratory and space experiments related to CIV have recently been reviewed extensively by Brenning.[2]

A few laboratory experiments have been conducted to study the CIV interactions, but their results cannot be easily scaled to space plasma problems, where the density and magnetic field are, up to a factor of 10^{10} and 10^6, respectively, lower than in the laboratory. Other problems facing laboratory investigations of CIV are the presence of walls or electrodes and the smallness of the ionization front,

*Paper 7I6, Bull. Am. Phys. Soc. **38**, 2042 (1993).
†Invited speaker.

 1070-664X/94/1(5)/1669/7/$6.00

TABLE I. Chronological list (1984–1993) of referenced PIC simulation models used for CIV studies and the effects considered by each. The effects are dimensionality, electromagnetic effects, ionizing, charge exchange, excitation and elastic collisions, real spatial dimensions, and real mass ratios.

Reference	11	12	16	13	14	7	15	6	This work
Year	84	85	86	88	88	90	90	92	93
Dimensions	1-D	1-D	1-D	$2\frac{1}{2}$-D	$2\frac{1}{2}$-D	1-D	1-D	1-D	$2\frac{1}{2}$-D
EM effects				√	√				
e^- impact ionization	√		√	√	√	√	√	√	√
Charge X collisions			√	√	√	√	√	√	√
e^- impact excitation			√	√	√	√	√		
Elastic scattering			√	√	√	√	√	√	
Real dimensions									√
Real m_i/m_e								√	√

which render the ionization region difficult for access by standard probing techniques.

The importance of the Earth's ionosphere and magnetosphere as an ideal laboratory to test the CIV phenomenon has been widely recognized in the past ten years.[3,4] Staging a CIV interaction in space can be an ideal way to study CIV under conditions closest to the scenario, in which the phenomenon was first hypothesized by Alfvén. In space, a relative motion between a gas and a plasma can be easily established by releasing a gas from an orbiting spacecraft or rocket, whose velocity with respect to the ionospheric plasma exceeds V_c. The ionization region can be made to have dimensions much larger than those of the spacecraft. The use of plasma diagnostics onboard satellites and subsatellites could allow for a thorough and parametric test of CIV.

There have been a few neutral gas injections in the ionosphere to study CIV using shaped charges released from sounding rockets.[5] In these rocket experiments the ionization yield (defined as the ratio of the number of produced ions to the total number of released neutrals, whose velocity exceeded V_c) was typically small and difficult to relate conclusively to CIV effects. The following two reasons for the low ionization yield of these experiments have been proposed in the literature: inefficient ion seeding of the neutral gas[6] (due to the low rate of charge exchange collisions[7]) and the shortness of the interaction time scale, which would produce small yields, even if CIV was operative.[5]

Neutral gas releases from orbiting spacecraft are more promising than rocket experiments for studying the parametric dependencies of a CIV interaction, since they allow the experiments to be repeated under various conditions.

Recently, CIV tests were made as part of the ATLAS-1 experiments conducted on the shuttle orbiter Atlantis on March 24, 1992. The neutral xenon releases on ATLAS-1 were shown[8] to satisfy many of the criteria thought to be necessary for a positive CIV test[9] and had the important advantage of a high mass flow rates (1.5 moles/s), which is also critical for producing enough ion seeds through charge exchange.[7]

The ATLAS-1 releases showed a factor of 60 increase in plasma density following each of the 100 ms long neutral xenon releases.[8] Wave activity in the lower hybrid band during the releases was also reported.[10]

The study of the ATLAS-1 tests can be enhanced by applying advanced numerical simulation codes that can handle realistic conditions of the experiments. In this paper we discuss a numerical simulation model developed specifically to study such neutral gas releases in the ionosphere. We present simulation results obtained by applying the code to the ATLAS-1 CIV tests using the actual release parameters reported in Ref. 8.

II. PREVIOUS NUMERICAL SIMULATIONS

Since 1984, particle-in-cell (PIC) codes have been used in the study of the CIV effect. The PIC simulations to date have clarified many aspects of the CIV effect, including the threshold aspect of the interaction,[11] suprathermal electron production,[12] the role of electromagnetic effects,[13] the presence of ionization fronts,[14] the importance of elastic scattering and the atomic physics such as charge exchange, excitation, and ionization from metastable states,[7,15,16] and the importance of initial ion seed in the neutral gas.[6]

Most of the simulations have been one dimensional, except for those in Refs. 13 and 14, in which two-dimensional simulations with artificial mass ratios were carried out using a small grid. Consequently, until now the simulations have been concerned with the investigation of fundamental aspects of CIV, and were not directly applied to any specific gas release experiment in space.

In order to model neutral gas releases in the ionosphere under realistic conditions we use a two-and-one-half-dimensional ($2\frac{1}{2}$-D) electrostatic PIC code that can handle real mass ratios and realistic spatial extensions. The effects included in the model are listed in Table I for comparison with those of previous simulation models. The present model neglects electromagnetic effects, since these were shown not to be important for the CIV interaction, when[13]

$$V < (1+\beta_e)^{1/2} v_A$$

(where V is the relative velocity, β_e is the electron beta, and v_A is the Alfvén velocity), a condition amply satisfied in most ionospheric release experiments. Although various collisional processes can be easily included and handled by the code, we limit the simulation discussed here to include only the most important ones, namely ionizing (electron impact) and charge exchange collisions.

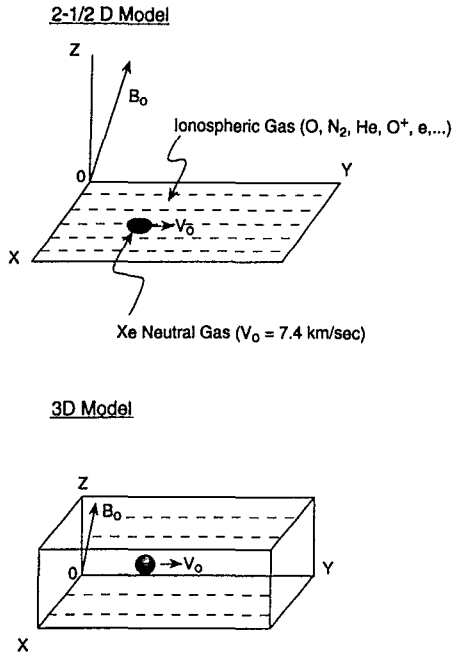

FIG. 1. Sketch of the numerical simulation models developed to study neutral gas release experiments into the ionosphere. A two-and-one-half-dimensional model (top) has two spatial coordinates, x and y, and three velocity components. Extension to a three-dimensional model (bottom) is straightforward.

III. SIMULATION MODEL

Shown in Fig. 1 is a sketch of the particle simulation model developed specifically for studying the neutral gas release experiments into the ionosphere. The model is two-and-one-half-dimensional in which two spatial coordinates, x and y, and three velocity components are followed in time. Full dynamics of the ions are followed in time, while the electrons are treated as guiding center particles, where rapid gyration around the guiding center has been averaged out. This averaging is tolerable for our case because we are not interested in the high-frequency electron gyromotion, and at the same time it allows us to use a larger integration time step, which is essential for simulations using realistic plasma parameters.[17] The code follows the motion of the background and ionized plasmas in a given uniform magnetic field representing the geomagnetic field and a self-consistent electrostatic field. Extension to the full three dimensions is straightforward by using higher-order interpolation to simulate a large three-dimensional volume.[18]

Using the Langmuir probe measurements for the ATLAS-1 releases reported in Ref. 8, we set the background oxygen ion density at 5×10^4 cm^{-3}, and the temperature at 0.1 eV. We also set the magnetic field strength at 0.7 G and the pitch angle of the velocity vector at 81°, as was the case for the actual releases. Main components of the background neutral gases are O and N_2, whose densities are 10^7–10^8/cm^3. The Debye length is typically 1 cm and the electron plasma and gyrofrequencies are about 10^7/s. The oxygen ion plasma frequency that is close to the lower hybrid frequency is about equal to 5.8×10^4/s.

The mass flow rate of 1.5 moles/s of the ATLAS-1 releases, which lasted 100 ms each, is equivalent to 10^{23} particles for a typical release. The reported observations suggest that a rapid ionization took place within a few ms.[8]

The interaction of the neutral xenon gas with the background plasma is treated by means of the Monte Carlo technique,[19] including charge exchange,

$$X_e+O^+=X_e^++O,$$

and electron impact ionization,

$$X_e+e=X_e^++2e.$$

The cross section for the oxygen–xenon charge exchange is 10^{-16} cm^2 at 10 eV energy and increases to 2×10^{-15} cm^2 at 100 eV.[20] The ionization energy of the ground state xenon atom is 12.13 eV and the dependence of the cross section for electron impact ionization on the energy is described in Ref. 21 and is shown to increase almost linearly from threshold, reaching the maximum of 6.2×10^{-16} cm^2 at 120 eV then decreasing to about 2×10^{-16} cm^2 at 1 keV.

In the simulation discussed here, we did not include other binary interactions, which could be added to the code. Among such interactions are line excitation, ionization from the ($6s$) metastable state, which can have cross sections as large as 10^{-14} cm^2 and elastic scattering of the X_e^+ ions by the xenon and oxygen neutral gases. These collisional effects will be included in a future simulation.

The dimensions of the simulation grid, shown in Fig. 1, are set to either $256(x)\times512(y)$ or $256(x)\times1024(y)$, which, for our particular case with the Debye length of 1 cm, correspond to either 256×512 cm or 256×1024 cm in real dimensions after setting the grid size equal to the Debye length.

Since the space shuttle and hence the neutral xenon gas are moving at 7.4 km/s orbital speed in the y direction, our simulation system is therefore traversed in 1.4 ms, unless the system length is stretched in the y direction.

The ATLAS-1 space observations[8] show, however, that a significant enhancement of ionization takes place within that time scale, so that the present simulation is large enough to study at least the initial stage of the interaction.

As mentioned earlier, real mass ratios are used for the electrons, oxygen, and xenon ions. The time step of integration used in the simulation was $(1–2)\omega_{pe}^{-1}$, which corresponds to $(1–2)\times10^{-7}$ s. While the detailed shape of the xenon gas is not known, we shall assume in our model that it is a sphere with a uniform density moving at the shuttle speed in the ionosphere. Since the xenon gas expansion speed of 61 m/s is much lower than the 7.4 km/s orbital speed, the changes in the radius and the density during the simulation were ignored.

The boundary conditions for the particles and field are the following. First, the background ionospheric oxygen ions and electrons, which are assumed uniform initially, are assumed periodic. The ionospheric ions, for example, leaving a boundary, are inserted back from the opposite

boundary. This is roughly equivalent to an assumption of a vast ionospheric background. The xenon ions produced by the impact ionization and charge exchange are assumed lost once they leave the boundary of the simulation. High-energy electrons accelerated by the plasma waves are also considered lost once they cross the simulation boundaries. The ideal boundary conditions for the electrostatic potential would be such that the potential vanishes at a point where the distance from the xenon cloud is far enough. This can be approximated by using a sine Fourier transform for the system, which sets the values of the potential at the boundary zero. As the waves grow to large amplitude at a later phase of the simulation, however, the plasma waves reach the boundary without much attenuation, so that some of the waves are reflected. In fact, the use of the periodic boundary condition gives results not much different from those that would be obtained using the sine Fourier transform. This is because the largest wave amplitude in the system remains concentrated near the xenon cloud.

In the example given below, we shall assume that the neutral xenon gas has a density of $3\times10^{14}/\mathrm{cm}^3$ with its radius of 8 cm. This would correspond to an early phase of the gas release.

The resulting evolution of the beam instability, the formation of suprathermal tails, the wave emission, and the enhancement to ionization under the above listed conditions are described by the simulation results in the next section.

IV. SIMULATION RESULTS

The released xenon neutrals have effectively the spacecraft orbital velocity of 7.4 km/s, and can undergo charge exchange with the background oxygen ions, resulting in an energetic xenon ion beam. Such a xenon ion beam is able to excite plasma waves near the oxygen lower hybrid and ion cyclotron waves propagating nearly perpendicular to the magnetic field. The lower hybrid and ion cyclotron waves, in turn, accelerate xenon ions perpendicular to the magnetic field and electrons along the magnetic field at roughly the same rate.[22] The energetic electrons, in turn, can enhance ionization of the xenon neutral gas, so that the original streaming energy of the neutral xenon is channeled through the waves to the ionization. The coupling of the lower hybrid wave to ions and electrons is comparable at an angle of propagation given by $k_{\|}/k_{\perp}=(m_e/m_i)^{1/2}$. If the angle is larger than this value, more energy is fed into the electrons, thus enhancing ionization. The threshold ion beam velocity, however, also increases with this angle.[22] This picture is upheld by the following simulation results.

Shown in Fig. 2 are the results of the simulation at $t=1000\omega_{pe}^{-1}$, which corresponds to approximately 0.1 ms. The electrostatic contour plot shown in panel (a) indicates a presence of potential fluctuations near the xenon cloud caused by the newly created xenon ions through a charge exchange. Since the neutral xenon density is high, the rate at which the xenon ions are created is substantial. The rate is given by $\sigma_c n_O + n_{X_e} V_r$, so that at $t=1$ ms the xenon ion density becomes comparable to the oxygen ion density near the xenon cloud. The potential fluctuations arise from the high-speed newly created xenon ions moving through the ionosphere. Here V_r is the relative speed between the neutral xenon gas and the oxygen ions.

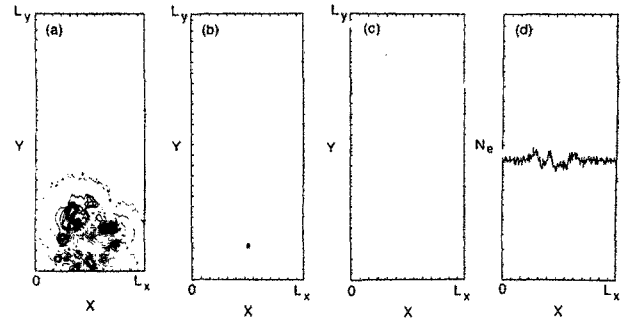

FIG. 2. Simulation results for a neutral gas cloud with a density of $3\times10^{14}/\mathrm{cm}^3$ and a radius of 8 cm at $t=0$ ms. Shown in the figure are electrostatic potential contours [panel (a)], location of the neutral xenon gas in the (x,y) plane [panel (b)], scatter plot of the ionospheric electrons [panel (c)], and the electron density averaged over the y direction [panel (d)]. At this early time of the simulation, the charge exchange process between the xenon neutral gas and the ionospheric oxygen ions produced a small number of xenon ions generating potential fluctuations near the xenon cloud. Local density perturbations can also be seen in panel (d).

Shown in panel (b) of Fig. 2 is the location of the xenon cloud moving at a speed of 7.4 km/s. As mentioned earlier, the cloud remains unchanged on the time scale of the simulation. A scatter plot of the ionospheric electron spatial distribution is shown in Fig. 2(c), which indicates that it is essentially uniform at this time. The average electron density shown in panel (d), however, indicates a presence of significant perturbations at the center of the system, where the xenon cloud is located. This perturbation is created by the newly created xenon ions trying to maintain the charge neutrality. The xenon ions are moving at high speed so that they tend to generate charges at the boundary, generating density perturbations as well as potential fluctuations shown in panels (a) and (d).

Shown in Fig. 3 are the corresponding distributions for

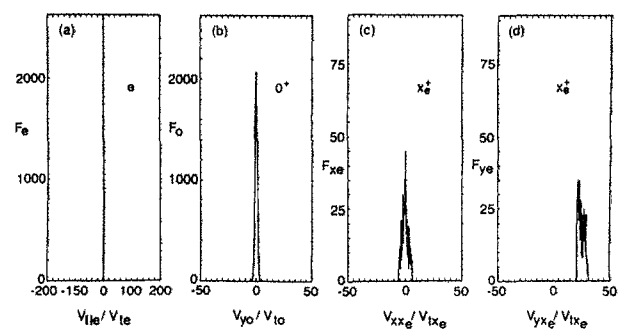

FIG. 3. Results of the same simulation as in Fig. 2, showing distributions for the electron velocity along the magnetic field [panel (a)], the oxygen ion perpendicular velocity V_y [panel (b)], the xenon ion perpendicular velocity V_x [panel (c)], and the associated V_y component [panel (d)]. Both the electrons and oxygen ions remain the same as the initial ionospheric distributions, while the xenon beam ions are created through charge exchange. Note the velocities are normalized by the thermal velocities of the corresponding species at the ionospheric temperature, 0.1 eV.

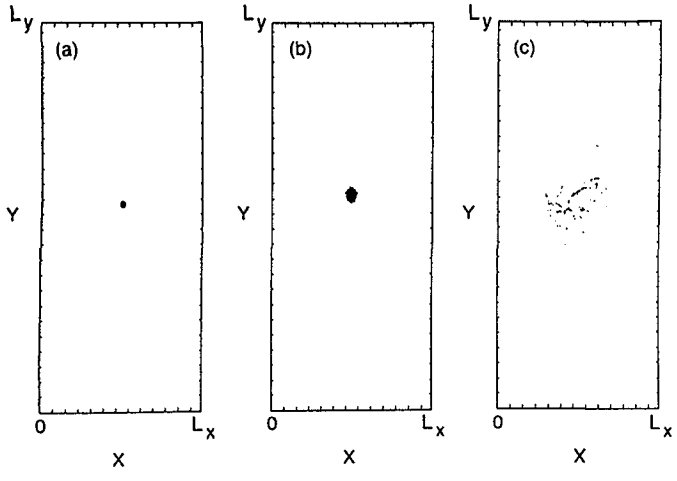

FIG. 4. Results for the location of the xenon neutral gas [panel (a)], scatter plots for the xenon ions [panel (b)], and for the newly created electrons [panel (c)] produced by electron impact ionization. Note the xenon ions move with the xenon neutral gas as expected, except for radial expansion, as shown in (b). The newly created electrons, on the other hand, spread out quickly from the neutral gas. Charge neutrality is maintained by the ionospheric oxygen ions and electrons.

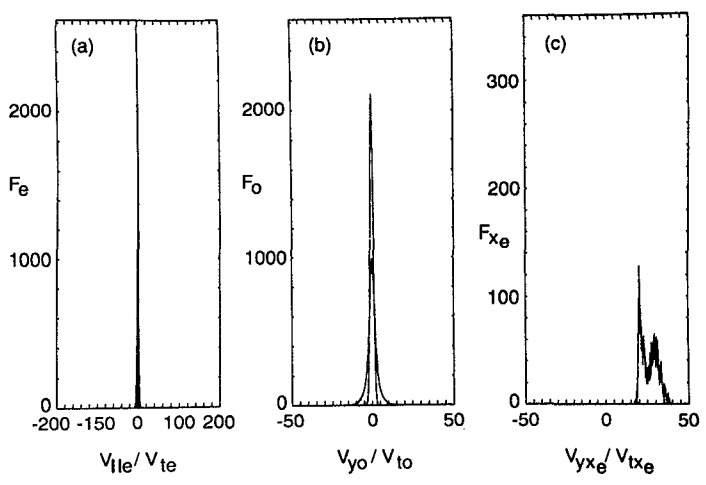

FIG. 5. The velocity distributions for the electrons [panel (a)], oxygen ions [panel (b)], and xenon ions [panel (c)] at $t=0.4$ ms. It is shown that acceleration of the electrons along and oxygen ions across the magnetic field began to take place as a result of the plasma instability near the oxygen lower hybrid waves. The delta-function-like distributions in panels (a) and (b) correspond to the initial electron and oxygen ion distributions at the ionospheric temperature.

the electron velocity along magnetic field [panel (a)], the oxygen ion perpendicular velocity V_y [panel (b)], the xenon ion perpendicular velocity V_x [panel (c)], and the associated V_y component [panel (d)]. Since the time is still short for the lower hybrid waves to grow, electrons and oxygen ion distributions are essentially the same as the initial ionospheric distributions at 0.1 eV. The xenon ions produced by the charge exchange process are streaming at the orbital speed. Note that the velocities shown in Fig. 3 are normalized by the thermal velocities of the corresponding species at the ionospheric temperature.

Shown in Fig. 4 are the results of the simulation at $t=0.4$ ms for the location of the xenon neutral gas [panel (a)], scatter plots for the xenon ions [panel (b)], and for the newly created electrons [panel (c)] produced by electron impact ionization. The xenon neutral cloud has moved farther across the magnetic field. The xenon ions also move with the orbital speed, together with the xenon neutral gas. The xenon ions, however, spread radially as they gyrate out from within the cloud. The newly created electrons spread out rapidly, as seen in Fig. 4(c), owing to their large mobility. The charge neutrality is maintained by the background ionospheric oxygen ions and electrons, whose densities are much higher than the newly created electrons at this time. We note that at this time the number of the xenon ions produced by charge exchange is much larger than the electron impact produced xenon ions (the ratio is 100 to 1). This is because there are very few high-energy electrons produced at this time.

Shown in Fig. 5 are the corresponding velocity distributions for the electrons [panel (a)], oxygen ions [panel (b)], and xenon ions [panel (c)] at this time (0.4 ms). It is clear that both the electrons and oxygen ions are accelerated somewhat from their initial ionospheric distributions, which are also included in panels (a) and (b). The xenon ion beam plotted in panel (c) shows a slowing down from the orbital speed, and, at the same time, a spreading caused by velocity space diffusion. The acceleration and diffusion of the particles are caused by plasma instabilities near the lower hybrid waves. The energy lost by the xenon ion beam is channeled to the acceleration of the electrons, which can, in turn, enhance the ionization of the neutral xenon gas substantially as the suprathermal electron population increases.

Shown in Fig. 6 is the power spectrum for a Fourier mode, $(m,n)=(4,3)$ [panel (a)], and the spectrum measured locally at a location near the xenon neutral cloud [panel (b)]. It is clearly seen that both spectra have a peak frequency near $2.0\omega_{po}$, which is close to the lower hybrid frequency, including the electron response.[22] This is direct evidence for the excitation of the oxygen lower hybrid waves by the xenon ion beam generated by the charge exchange process. The electrons accelerated by the lower

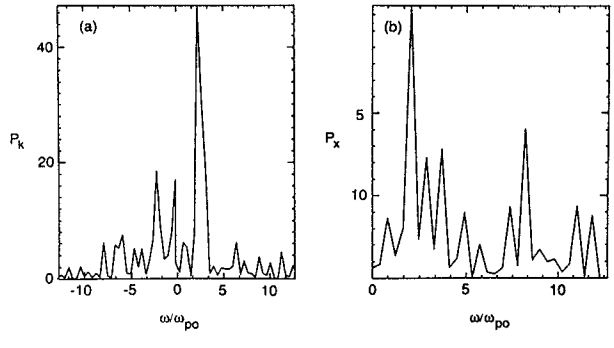

FIG. 6. Power spectra of the charge density for a Fourier mode $(m,n)=(4,3)$, (a), and at a location near the neutral gas in the (x,y) plane, (b). Note for both cases, a peak near $2.0\omega_{po}$ is clearly seen, which corresponds to the oxygen lower hybrid wave.

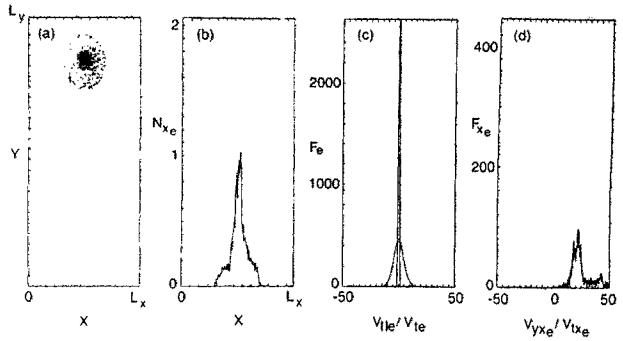

FIG. 7. Results of the simulation at $t=0.7$ ms for the xenon ion cloud produced by the electron impact in the (x,y) space [panel (a)], its average density in x [panel (b)], the electron velocity distribution [panel (c)], and the xenon ion velocity distribution [panel (d)].

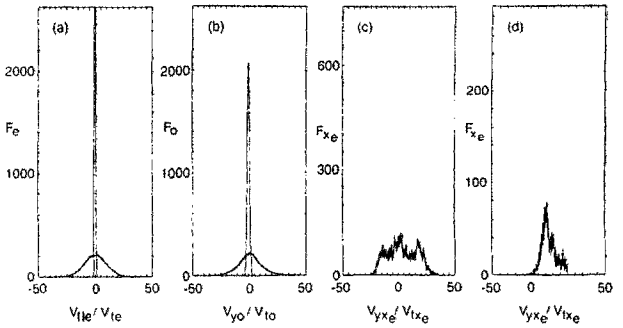

FIG. 8. Results of the simulation at $t=1$ ms for the velocity distributions of the electrons [panel (a)], oxygen ions [panel (b)], electron impact produced xenon ions [panel (c)], and charge exchange produced xenon ions [panel (d)].

hybrid waves, in turn, should increase the impact ionization, leading to further enhancement of the instability and a self-sustaining collective ionization process.

Shown in Fig. 7 are the results of the simulation at $t=0.7$ ms. The spatial distribution of xenon ions produced by electron impact ionization is shown in panel (a). Note that the cloud expands radially as it moves with the shuttle orbital velocity. It is interesting to note that the center of the cloud has much higher density surrounded by the outer region at lower density. This is clearly shown in panel (b), where the average xenon ion density is shown as a function of x. The peak xenon ion density is located near the center of the xenon neutral cloud, and its density is a quarter of the ambient oxygen ion density. At this time the number of xenon ions produced by the electron impact exceeds the number of xenon ions produced through charge exchange with ionospheric ions. More on this point will be discussed later.

The electron velocity distribution is shown in panel (c) of the same figure at $t=0.7$ ms, together with the initial ionospheric electron distribution. It is clear that the tail electrons are much hotter now, with a substantial portion having energies as high as 20 eV. Such electrons can indeed enhance the impact ionization of the neutral xenon gas because of both the enhanced density of electrons above the ionization threshold and the increase in the ionization cross section at these higher energies. The xenon ion Vy velocity distribution produced by the impact ionization is shown in panel (d). The drift speed is substantially smaller than the orbital speed, suggesting that the xenon kinetic energy associated with the orbital motion is channeled to the ionization as well as to the acceleration of various kinds of particles.

At $t=1$ ms, as shown in Fig. 8, the heating of the electrons and ionization of the xenon gas occur at a faster rate. The energy distribution of the electrons shown in panel (a) indicates a further suprathermal tail enhancement, with a substantial portion of the electrons having energies as high as 60 eV. The ionospheric oxygen ions shown in panel (b) is also heated substantially. The xenon ions produced by the impact ionization shown in panel (c) and by the charge exchange shown in panel (d) are accelerated, and at the same time their drift speed has decreased significantly. Note that the number of xenon ions produced by impact ionization is larger than the number of xenon ions produced through charge exchange by a factor of 3 at this time.

Shown in Fig. 9 is the time record of the xenon ions produced through charge exchange (open circles) and by electron impact ionization (solid circles). It is clear that the impact ionization, once it is triggered, increases much more rapidly than the charge exchange ionization, which is more or less linear in time. Since the impact ionization depends on the high-energy electron population, it is essential to accurately follow the development of the electron distribution by means of self-consistent means such as by the PIC simulation reported in this work. The electron

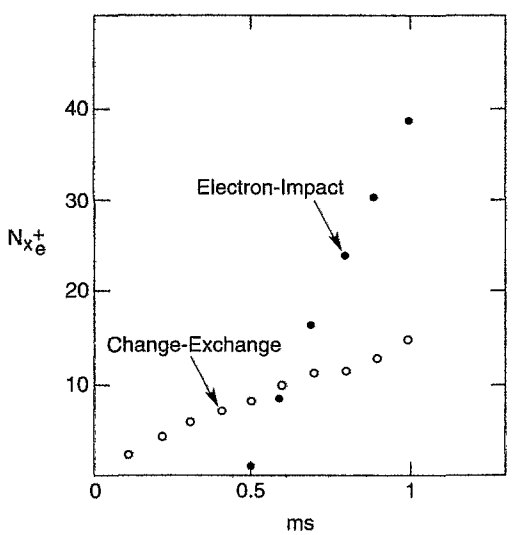

FIG. 9. Time record for the charge exchange produced xenon ions (open circles) and electron impact produced xenon ions (solid circles). The average xenon ion density is normalized by the average ionospheric plasma density, assuming that the total xenon ions are confined within the initial xenon neutral cloud. It is shown that the ionization produced xenon ions obtained a density as much as 30 times of the background oxygen ion density if there were no xenon ion diffusion in space. As discussed in the text, xenon ions actually diffused out radially, reducing its density comparable to the oxygen ion density at $t=1$ ms.

impact ionization completely dominates over charge exchange ionization after a few hundred microseconds into the simulation, demonstrating that an anomalous process such as CIV could indeed be important during neutral gas release experiments in space, in general, and the ATLAS-1 xenon releases, in particular.

IV. CONCLUDING REMARKS

We have shown that a simulation model developed to simulate neutral gas release experiments in the ionosphere can be used to study various physical processes associated with such space experiments, and determine the extent and importance of collective effects in ionization. The model was applied to the xenon gas release experiments conducted during the ATLAS-1 mission. The model still does not include all the subsidiary binary reactions (line excitation and radiation, elastic collisions, stripping ionization, and multiple ionization), which will be added in future simulations. It has been shown, however, how xenon ions, created from the released gas through charge exchange with ionospheric ions and streaming with a velocity exceeding V_c, can drive plasma waves near the lower hybrid frequency unstable, which can produce suprathermal electrons that can, in turn, lead to a rapid ionization of the neutral gas. This is essentially the CIV effect.

The number of xenon ions produced through the collective (CIV) effect (i.e., by the impact with suprathermal electrons accelerated by the waves) increases much more rapidly than the number of ions created through classical charge exchange ionization. This is in contrast with the finding in Ref. 23, where a quenching of the CIV effect was expected to occur when the CIV ionization rate becomes comparable with the charge exchange rate.

While our numerical simulation followed the evolution of the xenon gas release only to about 1 ms time, the total number density of the xenon ions produced by CIV and charge exchange becomes already comparable to the density of the ionospheric oxygen ions. With longer simulations, we expect the xenon ions produced through the CIV effect to keep on increasing rapidly, so that their density can far exceed the oxygen ion density within a relatively short period of time.

Since we found that, for the ATLAS-1 release conditions, CIV ionization dominates over charge exchange after only a short time (a few hundred microseconds), and since the observations show an increase of the density of a factor of 60 a few milliseconds into the release,[8] it seems likely that this density enhancement can be attributed to the CIV effect. This would be ascertained more quantitatively when all the relevant subsidiary reactions, such as elastic collisions of the beam ions and electrons with the neutrals, are included in the model. Finally, we plan to extend the simulations into full three dimensions, so that the three-dimensional structure of the neutral gas can be reflected in the model realistically.

ACKNOWLEDGMENTS

The authors would like to thank Dr. Shu T. Lai and Dr. Jill Marshall for stimulating discussions and useful information.

This work was supported by Air Force Office of Scientific Research Grant No. F49620-93-1-0222 and by U.S. Department of Energy Contract No. DE-AC02-76-CHO-3073 to Princeton University.

[1] H. Alfvén, Rev. Mod. Phys. **32**, 710 (1960).
[2] N. Brenning, Space Sci. Rev. **59**, 209 (1992).
[3] E. Möbius, R. W. Boswell, A. Piel, and D. Henry, Geoph. Res. Lett. **6**, 29 (1979).
[4] I. Axnäs, Geoph. Res. Lett. **7**, 933 (1980).
[5] R. B. Torbert, Adv. Space Res. **10**, 47 (1990).
[6] R. J. Biasca, Ph.D. thesis, Massachusetts Institute of Technology, Cambridge, MA, 1992.
[7] J. D. Person, H. Resendes, and D. Hastings, J. Geophy. Res. **95**, 4039 (1990).
[8] J. A. Marshall, J. L. Burch, E. Y. Choueiri, and N. Kawashima, Geophys. Res. Lett. **20**, 499 (1993).
[9] S. T. Lai and E. Murad, IEEE Trans. Plas. Sci. **PS-20**, 770 (1992).
[10] E. Y. Choueiri, J. A. Marshall, J. L. Burch, H. Okuda, and N. Kawashima, EOS **74**, 233 (1993).
[11] S. Machida, T. Abe, and T. Terasawa, Phys. Fluids **27**, 1928 (1984).
[12] T. Abe and S. Machida, Phys. Fluids **28**, 1178 (1985).
[13] S. Machida and C. Goertz, J. Geophys. Res. **93**, 11 495 (1988).
[14] S. Machida, C. Goertz, and G. Lu, J. Geomagn. Geoelect. **40**, 1205 (1988).
[15] W. McNeil, S. Lai, and E. Murad, J. Geophys. Res. **95**, 10345 (1990).
[16] S. Machida and C. K. Goertz, J. Geophy. Res. **11**, 11 965 (1986).
[17] W. W. Lee and H. Okuda, J. Comput. Phys. **17**, 139 (1978).
[18] H. Okuda, W. W. Lee, and C. Z. Cheng, Comput. Phys. Commun. **26**, 233 (1979).
[19] See, for example, C. K. Birdsall, IEEE Trans. Plasma Sci. **PS-19**, 65 (1991).
[20] M. Matic, V. Sadis, M. Vujovic, and B. Cobic, J. Phys. B Atom Mol. Phys. **13**, 3665 (1980).
[21] D. Rapp and P. Englander-Golden, J. Chem. Phys. **43**, 1464 (1965).
[22] J. M. Kindel, H. Okuda, and J. M. Dawson, Phys. Rev. Lett. **29**, 995 (1972).
[23] E. Moghaddam-Taaheri and C. K. Goertz, J. Geophys. Res. A **98**, 1443 (1993).